



Semnan University

Mechanics of Advanced Composite Structures

journal homepage: <http://MACS.journals.semnan.ac.ir>

Buckling Analysis of Nano Composite Plates Based on Combination of the Incremental Load Technique and Dynamic Relaxation Method

V. Zeighami ^a, M.E. Golmakani ^{a*}

^a Department of Mechanical Engineering, Mashhad Branch, Islamic Azad University, Mashhad, Iran

KEYWORDS

CNTRC plate
Buckling
Incremental loading
DR method

ABSTRACT

In this paper, a different method, incremental load technique in conjunction with dynamic relaxation (DR) method, is employed to analyze the buckling behavior of composite plates reinforced with functionally graded (FG) distributions of single-walled carbon nanotubes (SWCNTs) along the thickness direction. The properties of carbon-nanotubes reinforced composite (CNTRC) plate were determined through modified rule of mixture. The nonlinear governing relations are obtained incrementally in the form of partial differential equations (PDEs) based on first-order shear deformation theory (FSDT) and Von Karman nonlinear strain. In the proposed method, for finding the critical buckling load, the mechanical loads are applied to the CNTRC plate incrementally so that in each load step the incremental form of PDEs are solved by the DR method combined with the finite difference (FD) discretization technique. Finally, the critical buckling load is determined from the load-displacement curve. In order to verify the accuracy of the present method, the results are compared with those available in the literatures. Finally, a detailed parametric study is carried out and results demonstrate that the change of carbon nanotube volume fraction, plate width-to-thickness ratio, plate aspect ratio, boundary condition and loading condition have pronounced effects on the buckling strength of CNTRC plates. It is seen that for all types of loading, boundary conditions and both cases of with and without presence of elastic foundation the FG-X and FG-O have the highest and lowest values of buckling loads.

1. Introduction

Carbon nanotubes (CNTs) have been widely accepted owing to their remarkable mechanical, electrical and thermal properties and the applications of CNTs are thus drawing much attention currently. Conventional fiber-reinforced composite materials are normally made of stiff and strong fillers with microscale diameters embedded into various matrix phases.

The discovery of CNTs may lead to a new way to improve the properties of resulting composites by changing reinforcement phases to nano-scaled fillers [1]. Carbon nanotubes are considered as a potential candidate for the reinforcement of polymer composites, provided that good interfacial bonding between CNTs and polymer and proper dispersion of the individual CNTs in the polymeric matrix can be guaranteed [2]. Since

the load transfer between the nanotube and the matrix is less than perfect, several micromechanical models have been developed to predict properties of CNT-reinforced nanocomposites. Fidelus et al. [3] examined thermo-mechanical properties of epoxy-based nanocomposites with low weight fractions of randomly oriented single- and multi-walled carbon nanotubes with a rule-of-mixture type prediction of the modulus. Based on the rule of mixture, Anumandla and Gibson [4] presented a comprehensive closed form micromechanics model for estimating the elastic modulus of nanotube-reinforced composites. Han and Elliot [5] presented classical molecular dynamics (MD) simulations to model polymer/CNT composites constructed by embedding a single wall (10, 10) CNT into two different amorphous polymer matrices. The CNT-polymer interfacial shear

* Corresponding author. Tel.: +98-51-36625046; Fax: +98-51-36612960
E-mail address: m.e.golmakani@mshdiau.ac.ir

strength was determined according to a series of pull-out tests of individual carbon nanotubes embedded within polymer matrix by Wagner et al. [6,7], which demonstrated that carbon nanotubes are effective in reinforcing a polymer due to remarkably high separation stress. Molecular dynamics (MD) simulations were performed to predict the interfacial bonding by considering three-dimensional cross-links and stronger interfacial adhesion can be achieved through functionalization of the nanotube surface to form chemical bonding to the chains of polymer matrix [8,9]. Another fundamental issue is the dispersion of carbon nanotubes in the matrix, since CNTs tend to agglomerate and entangle because of their enormous surface area and high aspect ratio. Amino-functionalized CNTs are therefore developed to improve their dispersion in polymer resins [10]. The constitutive models and mechanical properties of carbon nanotube polymer composites have been studied analytically, experimentally, and numerically. A review and comparisons of mechanical properties of single- and multi-walled carbon nanotube reinforced composites fabricated by various processes were given by Coleman et al. [11]. In actual structural applications, carbon nanotube-reinforced composites (CNTRC), as a type of advanced material, may be incorporated in the form of beams, plates or shells as structural components. It is thus of importance to explore mechanical responses of the structures made of CNTRC. Wuite and Adali [12] firstly used the classical laminated beam theory to analyze symmetric cross-ply and angle-ply laminated beams stacked with multiple transversely isotropic layers reinforced by CNTs based on micromechanical constitutive models developed according to the Mori-Tanaka method. Vodenitcharova and Zhang [13] developed a continuum model for pure bending of a straight nanocomposite beam with a circular cross section reinforced by a single-walled carbon nanotube. Formica et al. [14] studied vibration behaviors of cantilevered CNTRC plates by employing an equivalent continuum model according to the Mori-Tanaka scheme. The buckling behaviors of laminated composite plates reinforced by SWCNTs were investigated analytically and numerically based on the classical laminated plate theory and third-order shear deformation theory, respectively, to consider the optimized orientation of CNTs for obtaining the highest critical load and corresponding mode shape were calculated for different kinds of boundary conditions as well as aspect ratios of the plates [15]. Motivated by the concept of functionally graded materials (FGM), Shen [16] suggested that for CNT-based composite structures the distributions of CNTs

within an isotropic matrix were designed purposefully to grade with certain rules along desired directions for the improvement of the mechanical properties of the structures and the nonlinear bending behaviors of the resulting functionally graded CNT-reinforced composite (FG-CNTRC) plates in thermal environments were presented. Zhu et al. [17] discovered that CNT reinforcements distributed close to top and bottom are more efficient than those distributed near the mid-plane for increasing the stiffness of CNTRC plates. Based on the Timoshenko beam theory, non-linear free vibrations of functionally graded CNTRC beams were analyzed with the Ritz method and direct iterative technique by Ke et al. [18]. They found linear and non-linear frequencies of FG-CNTRC beam with symmetrical distribution of CNTs are higher than those of beams with uniform or asymmetrical distribution of CNTs. By using a multi-scale approach, Shen and Zhang [19] discussed thermal buckling and post buckling behaviors of functionally graded nanocomposite plates reinforced by SWCNTs subjected to in-plane temperature variation. Aref et al [20, 21] investigated Higher-Order Thermo-Elastic Analysis of FG-CNTRC Cylindrical Vessels Surrounded by a Pasternak Foundation and Two-Dimensional Electro-Elastic Analysis of FG-CNTRC Cylindrical Laminated Pressure Vessels with Piezoelectric Layers Based on Third-Order Shear Deformation Theory. Based on a higher order shear deformation plate theory, nonlinear vibration of FG-SWCNT plates rested on elastic foundation in thermal environments was investigated by an improved perturbation technique [22]. Aref et al [23] investigated Effect of characteristics and distribution of porosity on electro-elastic analysis of laminated vessels with piezoelectric face-sheets based on higher-order modeling.

In the present study, a different method, incremental load technique in conjunction with dynamic relaxation (DR) method, is used to study the buckling of single-walled carbon nanotube reinforced composite plates resting on an elastic foundation and subjected to different tensile-compressive loads. A uniform and three kinds of functionally graded distributions of CNTs along the thickness direction of plate are considered. The properties of composite material in each point were determined by modified rule of mixture. All governing equations were obtained incrementally based on first order shear deformation theory (FSTD) and Von Karman nonlinear strains. Using the principle of minimum potential energy, the set of coupled nonlinear equilibrium equations was obtained in incremental form for different boundary conditions. The dynamic relaxation (DR) method combined with the finite difference discretization

technique is employed to find the critical buckling load for simply supported and clamped boundary conditions. To verify the present results and formulations, some comparison studies are carried out between the obtained results and the available solutions in the literature. Excellent agreement between the obtained and available results is observed. A detailed parametric study is carried out to investigate the effects of volume fraction of nanotubes, arrangement of nanotubes, width-to-thickness ratio, elastic foundation and aspect ratio on the buckling load of nanocomposite plates with clamped and simply supported boundary conditions.

2. Theoretical Formulations

2.1. Geometries of Problem

Fig. 1 shows the coordinate system, geometry and loadings of nanocomposite plate with different distributions of CNTs. The reinforced composite plates have four different distributions of nanotubes with definite length a , width b and thickness h .

2.2. Material Properties of Carbon Nanotube Reinforced Composites

In the present work, based on the modified rule of mixture and introducing the CNT efficiency parameters the effective material properties (elastic modulus and Poisson ratios) of CNTRC plate can be expressed as follows [16]:

$$E_{11} = \eta_1 V_{CNT} E_{11}^{CNT} + V_m E_m \quad (1)$$

$$\frac{\eta_2}{E_{22}} = \frac{V_{CNT}}{E_{22}^{CNT}} + \frac{V_m}{E_m} \quad (2)$$

$$\frac{\eta_3}{G_{12}} = \frac{V_{CNT}}{G_{12}^{CNT}} + \frac{V_m}{G_m} \quad (3)$$

Where E_{11}^{CNT} , E_{22}^{CNT} , and G_{12}^{CNT} refer to elasticity modulus and shear modulus of carbon nanotubes, respectively. Also, E_m and G_m indicate the elasticity modulus and shear modulus of the substrate and $\eta_j = (1,2,3)$ is the CNT efficiency parameters which is introduced by Shen [16] for accounting the small-scale effect and other effects on the material properties of CNTRCs. The values of η_j is determined by matching the elastic moduli of CNTRCs predicted by the molecular dynamics (MD) simulations with those obtained from the modified rule of mixture in Eqs. (1) - (3). Furthermore, V_{CNT} and V_m are volume fractions of carbon nanotubes and substrate, respectively, and expressed as follows:

$$V_{CNT} + V_m = 1 \quad (4)$$

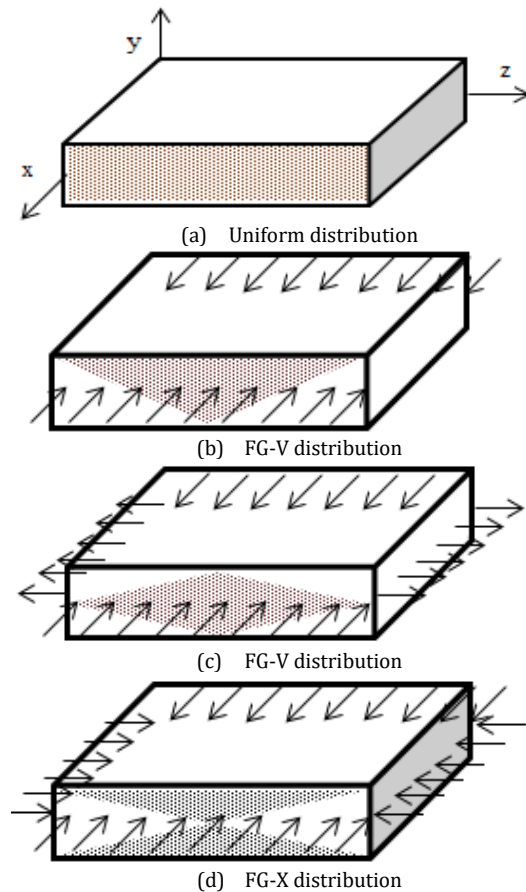


Fig. 1. Nano-composite plates subjected to various types of loading with (a) uniform, (b) FG-V, (c) FG-O and (d) FG-X distributions of CNTs.

The volume fraction of the uniform and three types of functionally graded distributions of the carbon nanotubes is determined through following expressions [17].

$$\begin{aligned} V_{CNT}(z) &= V_{CNT}^* && \text{(UD-CNTRC)} \\ V_{CNT}(z) &= \left(1 + \frac{2Z}{h}\right) V_{CNT}^* && \text{(FG-V CNTRC)} \\ V_{CNT}(z) &= 2 \left(1 - \frac{2|Z|}{h}\right) V_{CNT}^* && \text{(FG-O CNTRC)} \\ V_{CNT}(z) &= 2 \left(\frac{2|Z|}{h}\right) V_{CNT}^* && \text{(FG-X CNTRC)} \end{aligned} \quad (5)$$

So that

$$V_{CNT}^* = \frac{w_{CNT}}{w_{CNT} + \left(\frac{\rho^{CNT}}{\rho^m}\right) - \left(\frac{\rho^{CNT}}{\rho^m}\right) w_{CNT}} \quad (6)$$

Where w_{CNT} is the mass fraction of carbon nanotubes in composite plate. In above expressions, ρ^m and ρ^{CNT} refer to densities of substrate and carbon nanotubes, respectively. It is noticed that the four types of CNTRC plates possess the same mass fraction (w_{CNT}) and volume of CNTs. According to the following

relation, Poisson’s ratio, ν_{12} , is assumed to be uniformly distributed over the thickness of the functionally graded CNTRC plates.

$$\nu_{12} = V_{CNT}^* \nu_{12}^{CNT} + V_m \nu_m^m \tag{7}$$

2.3. Governing equations

The first-order shear deformation theory (FSDT) is employed to predict the displacement field $\{u, v, w\}^T$ of CNTRC plate. Based on FSDT, the displacement field is expressed as follows [24].

$$\begin{Bmatrix} u(x, y) \\ v(x, y) \\ w(x, y) \end{Bmatrix} = \begin{Bmatrix} u_0(x, y) \\ v_0(x, y) \\ w_0(x, y) \end{Bmatrix} + z \begin{Bmatrix} \psi_x(x, y) \\ \psi_y(x, y) \\ 0 \end{Bmatrix} \tag{8}$$

Where u_0 , v_0 and w_0 denote displacement components of the mid-plane in the x , y and z directions, respectively. Moreover, ψ_x and ψ_y represent rotations of a transverse normal about y and x axes, respectively. In order to predict the buckling load by the DR method the equilibrium equations should be derived in the incremental form. Thus, all of the following governing equations are derived in the incremental form of variables. By assuming small strains and moderate rotations, based on the incremental nonlinear von Karman strain-displacement relations, the strain components associated with the displacement field of Eq. (8) are expressed as follows [24]:

$$\begin{Bmatrix} \delta \varepsilon_{xx} \\ \delta \varepsilon_{yy} \\ \delta \gamma_{xy} \\ \delta \gamma_{yz} \\ \delta \gamma_{xz} \end{Bmatrix} = \begin{Bmatrix} \delta \varepsilon_{xx}^0 \\ \delta \varepsilon_{yy}^0 \\ \delta \gamma_{xy}^0 \\ \delta \gamma_{yz}^0 \\ \delta \gamma_{xzy}^0 \end{Bmatrix} + z \begin{Bmatrix} \delta k_{xx} \\ \delta k_{yy} \\ 0 \\ 0 \\ 0 \end{Bmatrix} \tag{9}$$

In which

$$\begin{Bmatrix} \delta k_{xx} \\ \delta k_{yy} \\ \delta k_{xy} \end{Bmatrix} = \begin{Bmatrix} \frac{\partial \delta \psi_x}{\partial x} \\ \frac{\partial \delta \psi_y}{\partial y} \\ \frac{\partial \delta \psi_x}{\partial y} + \frac{\partial \delta \psi_y}{\partial x} \end{Bmatrix}$$

$$\begin{Bmatrix} \delta \varepsilon_{xx}^0 \\ \delta \varepsilon_{yy}^0 \\ \delta \gamma_{xy}^0 \\ \delta \gamma_{yz}^0 \\ \delta \gamma_{xzy}^0 \end{Bmatrix} = \begin{Bmatrix} \frac{\partial \delta u_0}{\partial x} + \frac{\partial w_0}{\partial x} \frac{\partial \delta w_0}{\partial x} + \frac{1}{2} \left(\frac{\partial \delta w_0}{\partial x} \right)^2 \\ \frac{\partial \delta v_0}{\partial y} + \frac{\partial w_0}{\partial y} \frac{\partial \delta w_0}{\partial y} + \frac{1}{2} \left(\frac{\partial \delta w_0}{\partial y} \right)^2 \\ \frac{\partial \delta u_0}{\partial y} + \frac{\partial \delta v_0}{\partial x} + \frac{\partial \delta w_0}{\partial x} \frac{\partial w_0}{\partial y} \\ + \frac{\partial w_0}{\partial x} \frac{\partial \delta w_0}{\partial y} + \frac{\partial \delta w_0}{\partial x} \frac{\partial \delta w_0}{\partial y} \\ \frac{\partial \delta w_0}{\partial y} + \delta \psi_y \\ \frac{\partial \delta w_0}{\partial x} + \delta \psi_x \end{Bmatrix} \tag{10}$$

According to the Hooke’s law, the incremental constitutive relations are defined as follows:

$$\begin{Bmatrix} \delta \sigma_{xx} \\ \delta \sigma_{yy} \\ \delta \sigma_{xy} \\ \delta \sigma_{yz} \\ \delta \sigma_{xz} \end{Bmatrix}^T = \begin{bmatrix} Q_{11}(z) & Q_{11}(z) & 0 & 0 & 0 \\ Q_{11}(z) & Q_{11}(z) & 0 & 0 & 0 \\ 0 & 0 & Q_{11}(z) & 0 & 0 \\ 0 & 0 & 0 & Q_{11}(z) & 0 \\ 0 & 0 & 0 & 0 & Q_{11}(z) \end{bmatrix} \tag{11}$$

$$* \begin{Bmatrix} \delta \varepsilon_{xx} \\ \delta \varepsilon_{yy} \\ \delta \gamma_{xy} \\ \delta \gamma_{yz} \\ \delta \gamma_{xz} \end{Bmatrix}^T$$

In which the Q_{ij} components are defined by

$$Q_{11} = \frac{E_{11}}{1 - \nu_{12}\nu_{21}}, \quad Q_{22} = \frac{E_{22}}{1 - \nu_{12}\nu_{21}}$$

$$Q_{12} = \frac{\nu_{21}E_{11}}{1 - \nu_{12}\nu_{21}}, \quad Q_{66} = G_{12}, \tag{12}$$

$$Q_{44} = G_{23}, \quad Q_{55} = G_{13}$$

In above relations, E_{11} and E_{22} refer to elasticity moduli of CNTRC plate along x and y directions, respectively. In addition, G_{12} , G_{23} and G_{13} denote shear moduli and ν_{12} and ν_{21} refer to Poisson ratios. The incremental forces, moments and shear stress resultants can be expressed by the following expressions.

$$\begin{Bmatrix} \delta N_{xx} \\ \delta N_{yy} \\ \delta N_{xy} \end{Bmatrix} = \int_{-\frac{h}{2}}^{\frac{h}{2}} \begin{Bmatrix} \delta \sigma_{xx} \\ \delta \sigma_{yy} \\ \delta \sigma_{xy} \end{Bmatrix} dz,$$

$$\begin{Bmatrix} \delta M_{xx} \\ \delta M_{yy} \\ \delta M_{xy} \end{Bmatrix} = \int_{-\frac{h}{2}}^{\frac{h}{2}} \begin{Bmatrix} \delta \sigma_{xx} \\ \delta \sigma_{yy} \\ \delta \sigma_{xy} \end{Bmatrix} z dz, \tag{13}$$

$$\begin{Bmatrix} \delta Q_y \\ \delta Q_x \end{Bmatrix} = \int_{-\frac{h}{2}}^{\frac{h}{2}} \begin{Bmatrix} \delta \sigma_{yz} \\ \delta \sigma_{xz} \end{Bmatrix} dz$$

By substituting Eqs. (9) to (12) in Eq. (13), the incremental forces, moments and shear-stress resultants is obtained as follows

$$\begin{Bmatrix} \delta N_{xx} \\ \delta N_{yy} \\ \delta N_{xy} \end{Bmatrix} = \begin{bmatrix} A_{11} & A_{12} & 0 \\ A_{12} & A_{22} & 0 \\ 0 & 0 & A_{66} \end{bmatrix} \begin{Bmatrix} \delta \varepsilon_{xx}^0 \\ \delta \varepsilon_{yy}^0 \\ \delta \gamma_{xy}^0 \end{Bmatrix}$$

$$+ \begin{bmatrix} B_{11} & B_{12} & 0 \\ B_{12} & B_{22} & 0 \\ 0 & 0 & B_{66} \end{bmatrix} \begin{Bmatrix} \delta k_{xx} \\ \delta k_{yy} \\ \delta k_{xy} \end{Bmatrix} \tag{14}$$

$$\begin{Bmatrix} \delta M_{xx} \\ \delta M_{yy} \\ \delta M_{xy} \end{Bmatrix} = \begin{bmatrix} B_{11} & B_{12} & 0 \\ B_{12} & B_{22} & 0 \\ 0 & 0 & A_{66} \end{bmatrix} \begin{Bmatrix} \delta \varepsilon_{xx}^0 \\ \delta \varepsilon_{yy}^0 \\ \delta \gamma_{xy}^0 \end{Bmatrix} + \begin{bmatrix} D_{11} & D_{12} & 0 \\ D_{12} & D_{22} & 0 \\ 0 & 0 & D_{66} \end{bmatrix} \begin{Bmatrix} \delta k_{xx} \\ \delta k_{yy} \\ \delta k_{xy} \end{Bmatrix} \quad (15)$$

$$\begin{Bmatrix} \delta Q_y \\ \delta Q_x \end{Bmatrix} = \begin{bmatrix} A_{44}^s & 0 \\ 0 & A_{55}^s \end{bmatrix} \begin{Bmatrix} \delta \gamma_{yz}^0 \\ \delta \gamma_{xz}^0 \end{Bmatrix} \quad (16)$$

where A, B, D and A^s are the extensional, coupling, bending, and shear stiffness, respectively, which are obtained by the following expressions:

$$(A_{ij}, B_{ij}, D_{ij}) = \int_{-h/2}^{h/2} Q_{ij}(1, z, z^2) dz \quad (17)$$

$$A_{ij}^s = k_s \int_{-h/2}^{h/2} Q_{ij} dz \quad (18)$$

Where $i, j = 1, 2, 6$ and k_s is transverse shear correction coefficient that assumed to be $5/(6 - \nu_{12})$ along the thickness direction [17]. By substituting Eq. (10) in Eqs. (14) to (16), the incremental form of stress resultants can be obtained based on displacement field as follows:

$$\begin{aligned} \delta N_{xx} = & A_{11} \left(\frac{\partial \delta u_0}{\partial x} + \frac{\partial w_0}{\partial x} \frac{\partial \delta w_0}{\partial x} + \frac{1}{2} \left(\frac{\partial \delta w_0}{\partial x} \right)^2 \right) \\ & + B_{11} \frac{\partial \delta \psi_x}{\partial x} + B_{12} \frac{\partial \delta \psi_y}{\partial y} \\ & + A_{12} \left(\frac{\partial \delta v_0}{\partial y} + \frac{\partial w_0}{\partial y} \frac{\partial \delta w_0}{\partial y} + \frac{1}{2} \left(\frac{\partial \delta w_0}{\partial y} \right)^2 \right) \\ \delta N_{yy} = & A_{12} \left(\frac{\partial \delta u_0}{\partial x} + \frac{\partial w_0}{\partial x} \frac{\partial \delta w_0}{\partial x} + \frac{1}{2} \left(\frac{\partial \delta w_0}{\partial x} \right)^2 \right) \\ & + A_{22} \left(\frac{\partial \delta v_0}{\partial y} + \frac{\partial w_0}{\partial y} \frac{\partial \delta w_0}{\partial y} + \frac{1}{2} \left(\frac{\partial \delta w_0}{\partial y} \right)^2 \right) \\ & + B_{12} \frac{\partial \delta \psi_x}{\partial x} + B_{22} \frac{\partial \delta \psi_y}{\partial y} \\ \delta N_{xy} = & A_{66} \left(\frac{\partial \delta u_0}{\partial y} + \frac{\partial \delta v_0}{\partial x} + \frac{\partial w_0}{\partial y} \frac{\partial \delta w_0}{\partial x} \right. \\ & \left. + \frac{\partial \delta w_0}{\partial y} \frac{\partial w_0}{\partial x} + \frac{\partial \delta w_0}{\partial x} \frac{\partial \delta w_0}{\partial y} \right) \\ & + B_{66} \left(\frac{\partial \delta \psi_x}{\partial y} + \frac{\partial \delta \psi_y}{\partial x} \right) \end{aligned}$$

$$\begin{aligned} \delta M_{xx} = & B_{11} \left(\frac{\partial \delta u_0}{\partial x} + \frac{\partial w_0}{\partial x} \frac{\partial \delta w_0}{\partial x} \right. \\ & \left. + \frac{1}{2} \left(\frac{\partial \delta w_0}{\partial x} \right)^2 \right) \\ & + D_{11} \frac{\partial \delta \psi_x}{\partial x} + D_{12} \frac{\partial \delta \psi_y}{\partial y} \\ & + B_{12} \left(\frac{\partial \delta v_0}{\partial y} + \frac{\partial w_0}{\partial y} \frac{\partial \delta w_0}{\partial y} \right. \\ & \left. + \frac{1}{2} \left(\frac{\partial \delta w_0}{\partial y} \right)^2 \right) \\ \delta M_{yy} = & B_{12} \left(\frac{\partial \delta u_0}{\partial x} + \frac{\partial w_0}{\partial x} \frac{\partial \delta w_0}{\partial x} \right. \\ & \left. + \frac{1}{2} \left(\frac{\partial \delta w_0}{\partial x} \right)^2 \right) \\ & + D_{12} \frac{\partial \delta \psi_x}{\partial x} + D_{22} \frac{\partial \delta \psi_y}{\partial y} \\ & + B_{22} \left(\frac{\partial \delta v_0}{\partial y} + \frac{\partial w_0}{\partial y} \frac{\partial \delta w_0}{\partial y} \right. \\ & \left. + \frac{1}{2} \left(\frac{\partial \delta w_0}{\partial y} \right)^2 \right) \\ \delta M_{xy} = & B_{66} \left(\frac{\partial \delta u_0}{\partial y} + \frac{\partial \delta v_0}{\partial x} + \frac{\partial w_0}{\partial y} \frac{\partial \delta w_0}{\partial x} \right. \\ & \left. + \frac{\partial \delta w_0}{\partial y} \frac{\partial w_0}{\partial x} + \frac{\partial \delta w_0}{\partial x} \frac{\partial \delta w_0}{\partial y} \right) \\ & + D_{66} \left(\frac{\partial \delta \psi_x}{\partial y} + \frac{\partial \delta \psi_y}{\partial x} \right) \\ \delta Q_y = & A_{44} \left(\frac{\partial \delta w_0}{\partial y} + \delta \psi_y \right) + A_{45} \left(\frac{\partial \delta w_0}{\partial x} + \delta \psi_x \right) \\ \delta Q_x = & A_{55} \left(\frac{\partial \delta w_0}{\partial x} + \delta \psi_x \right) + A_{45} \left(\frac{\partial \delta w_0}{\partial y} + \delta \psi_y \right) \end{aligned} \quad (19)$$

Using the principle of minimum total potential energy, the equilibrium equations are obtained based on FSDT as follows:

$$\begin{aligned} \delta u_0 : & \frac{\partial \delta N_{xx}}{\partial x} + \frac{\partial \delta N_{xy}}{\partial y} = 0 \\ \delta v_0 : & \frac{\partial \delta N_{xy}}{\partial x} + \frac{\partial \delta N_{yy}}{\partial y} = 0 \\ \delta w_0 : & \frac{\partial \delta Q_x}{\partial x} + \frac{\partial \delta Q_y}{\partial y} + \delta N_{xx} \left(\frac{\partial^2 w}{\partial x^2} \right) \\ & + (N_{xx} + \delta N_{xx}) \frac{\partial^2 \delta w}{\partial x^2} \\ & + \delta N_{yy} \left(\frac{\partial^2 w}{\partial y^2} \right) + (N_{yy} + \delta N_{yy}) \frac{\partial^2 \delta w}{\partial y^2} \\ & + 2\delta N_{xy} \left(\frac{\partial^2 w}{\partial x \partial y} \right) + 2(N_{xy} + \delta N_{xy}) \frac{\partial^2 \delta w}{\partial x \partial y} \\ & - K_w \delta w + K_s \left(\frac{\partial^2 \delta w_0}{\partial x^2} + \frac{\partial^2 \delta w_0}{\partial y^2} \right) + \delta q_0 = 0 \end{aligned}$$

$$\begin{aligned} \delta\psi_x &: \frac{\partial \delta M_{xx}}{\partial x} + \frac{\partial \delta M_{xy}}{\partial y} - \delta Q_x = 0 \\ \delta\psi_y &: \frac{\partial \delta M_{xy}}{\partial x} + \frac{\partial \delta M_{yy}}{\partial y} - \delta Q_y = 0 \end{aligned} \tag{20}$$

In which, K_w and K_s are Winkler and shear coefficients of foundation parameters, respectively. It is noticed that incremental load δq_0 is the transverse mechanical load and must be removed from the third relation of Eq. (20) for the buckling analysis. By substituting Eq. (19) in Eq. (20), the equilibrium equations are obtained based on displacement field as follows

$$\begin{aligned} & \left(\begin{aligned} & A_{11} \left(\frac{\partial^2 \delta u_0}{\partial x^2} + \frac{\partial^2 w_0}{\partial x^2} \frac{\partial \delta w_0}{\partial x} \right) \\ & + A_{12} \left(\frac{\partial^2 \delta v_0}{\partial x \partial y} + \frac{\partial^2 w_0}{\partial x \partial y} \frac{\partial \delta w_0}{\partial y} \right) \\ & + A_{66} \left(\frac{\partial^2 \delta u_0}{\partial y^2} + \frac{\partial^2 \delta v_0}{\partial x \partial y} + \frac{\partial^2 \delta w_0}{\partial x \partial y} \frac{\partial w_0}{\partial y} \right. \\ & \quad \left. + \frac{\partial \delta w_0}{\partial x} \frac{\partial^2 w_0}{\partial y^2} + \frac{\partial^2 w_0}{\partial x \partial y} \frac{\partial \delta w_0}{\partial y} \right. \\ & \quad \left. + \frac{\partial w_0}{\partial x} \frac{\partial^2 \delta w_0}{\partial y^2} + \frac{\partial^2 \delta w_0}{\partial x \partial y} \frac{\partial \delta w_0}{\partial y} \right. \\ & \quad \left. + \frac{\partial \delta w_0}{\partial x} \frac{\partial^2 \delta w_0}{\partial y^2} \right) \\ & + B_{11} \frac{\partial^2 \delta \psi_x}{\partial x^2} + B_{12} \frac{\partial^2 \delta \psi_y}{\partial x \partial y} + B_{66} \left(\frac{\partial^2 \delta \psi_x}{\partial y^2} + \frac{\partial^2 \delta \psi_y}{\partial x \partial y} \right) = 0 \\ & \left(\begin{aligned} & A_{12} \left(\frac{\partial^2 \delta u_0}{\partial x \partial y} + \frac{\partial^2 w_0}{\partial x \partial y} \frac{\partial \delta w_0}{\partial x} \right) \\ & + \frac{\partial w_0}{\partial x} \frac{\partial^2 \delta w_0}{\partial x \partial y} + \frac{\partial \delta w_0}{\partial x} \frac{\partial^2 \delta w_0}{\partial x \partial y} \right) \\ & + A_{22} \left(\frac{\partial^2 \delta v_0}{\partial y^2} + \frac{\partial^2 w_0}{\partial y^2} \frac{\partial \delta w_0}{\partial y} \right) \\ & + \frac{\partial w_0}{\partial y} \frac{\partial^2 \delta w_0}{\partial y^2} + \frac{\partial \delta w_0}{\partial y} \frac{\partial^2 \delta w_0}{\partial y^2} \right) \\ & + A_{66} \left(\frac{\partial^2 \delta u_0}{\partial x \partial y} + \frac{\partial^2 \delta v_0}{\partial x^2} + \frac{\partial^2 \delta w_0}{\partial x^2} \frac{\partial w_0}{\partial y} \right. \\ & \quad \left. + \frac{\partial \delta w_0}{\partial x} \frac{\partial^2 w_0}{\partial x \partial y} + \frac{\partial^2 w_0}{\partial x^2} \frac{\partial \delta w_0}{\partial y} \right. \\ & \quad \left. + \frac{\partial w_0}{\partial x} \frac{\partial^2 \delta w_0}{\partial x \partial y} + \frac{\partial^2 \delta w_0}{\partial x^2} \frac{\partial \delta w_0}{\partial y} \right. \\ & \quad \left. + \frac{\partial \delta w_0}{\partial x} \frac{\partial^2 \delta w_0}{\partial x \partial y} \right) \\ & + B_{12} \frac{\partial^2 \delta \psi_x}{\partial x \partial y} + B_{22} \frac{\partial^2 \delta \psi_y}{\partial y^2} + B_{66} \left(\frac{\partial^2 \delta \psi_x}{\partial x \partial y} + \frac{\partial^2 \delta \psi_y}{\partial x^2} \right) = 0 \end{aligned} \right) \end{aligned}$$

$$\begin{aligned} & A_{55} \left(\frac{\partial^2 \delta w_0}{\partial x^2} + \frac{\partial \delta \psi_x}{\partial x} \right) + A_{45} \left(\frac{\partial^2 \delta w_0}{\partial x \partial y} + \frac{\partial \delta \psi_y}{\partial x} \right) \\ & + A_{44} \left(\frac{\partial^2 \delta w_0}{\partial y^2} + \frac{\partial \delta \psi_x}{\partial y} \right) + A_{45} \left(\frac{\partial^2 \delta w_0}{\partial x \partial y} + \frac{\partial \delta \psi_x}{\partial y} \right) \\ & \left(\begin{aligned} & A_{11} \left(\frac{\partial \delta u_0}{\partial x} + \frac{\partial w_0}{\partial x} \frac{\partial \delta w_0}{\partial x} + \frac{1}{2} \left(\frac{\partial \delta w_0}{\partial x} \right)^2 \right) \\ & + A_{12} \left(\frac{\partial \delta v_0}{\partial y} + \frac{\partial w_0}{\partial y} \frac{\partial \delta w_0}{\partial y} + \frac{1}{2} \left(\frac{\partial \delta w_0}{\partial y} \right)^2 \right) \right) \frac{\partial^2 w}{\partial x^2} \\ & + B_{11} \frac{\partial \delta \psi_x}{\partial x} + B_{12} \frac{\partial \delta \psi_y}{\partial y} \\ & \left(\begin{aligned} & A_{11} \left(\frac{\partial u_0}{\partial x} + \frac{1}{2} \left(\frac{\partial w_0}{\partial x} \right)^2 \right) + A_{12} \left(\frac{\partial v_0}{\partial y} \right. \\ & \quad \left. + \frac{1}{2} \left(\frac{\partial w_0}{\partial y} \right)^2 \right) \\ & + A_{11} \left(\frac{\partial \delta u_0}{\partial x} + \frac{\partial w_0}{\partial x} \frac{\partial \delta w_0}{\partial x} + \frac{1}{2} \left(\frac{\partial \delta w_0}{\partial x} \right)^2 \right) \\ & + A_{12} \left(\frac{\partial \delta v_0}{\partial y} + \frac{\partial w_0}{\partial y} \frac{\partial \delta w_0}{\partial y} + \frac{1}{2} \left(\frac{\partial \delta w_0}{\partial y} \right)^2 \right) \\ & + B_{11} \frac{\partial \psi_x}{\partial x} + B_{11} \frac{\partial \delta \psi_x}{\partial x} + B_{12} \frac{\partial \psi_y}{\partial y} + B_{12} \frac{\partial \delta \psi_y}{\partial y} \end{aligned} \right) \frac{\partial^2 w}{\partial x^2} \\ & \left(\begin{aligned} & A_{12} \left(\frac{\partial \delta u_0}{\partial x} + \frac{\partial w_0}{\partial x} \frac{\partial \delta w_0}{\partial x} + \frac{1}{2} \left(\frac{\partial \delta w_0}{\partial x} \right)^2 \right) \\ & + A_{22} \left(\frac{\partial \delta v_0}{\partial y} + \frac{\partial w_0}{\partial y} \frac{\partial \delta w_0}{\partial y} + \frac{1}{2} \left(\frac{\partial \delta w_0}{\partial y} \right)^2 \right) \\ & + B_{12} \frac{\partial \delta \psi_x}{\partial x} + B_{22} \frac{\partial \delta \psi_y}{\partial y} \end{aligned} \right) \frac{\partial^2 w}{\partial y^2} \\ & \left(\begin{aligned} & A_{12} \left(\frac{\partial u_0}{\partial x} + \frac{1}{2} \left(\frac{\partial w_0}{\partial x} \right)^2 \right) + A_{22} \left(\frac{\partial v_0}{\partial y} + \frac{1}{2} \left(\frac{\partial w_0}{\partial y} \right)^2 \right) \\ & + A_{12} \left(\frac{\partial \delta u_0}{\partial x} + \frac{\partial w_0}{\partial x} \frac{\partial \delta w_0}{\partial x} + \frac{1}{2} \left(\frac{\partial \delta w_0}{\partial x} \right)^2 \right) \\ & + A_{22} \left(\frac{\partial \delta v_0}{\partial y} + \frac{\partial w_0}{\partial y} \frac{\partial \delta w_0}{\partial y} + \frac{1}{2} \left(\frac{\partial \delta w_0}{\partial y} \right)^2 \right) \\ & + B_{12} \left(\frac{\partial \psi_x}{\partial x} \right) + B_{12} \left(\frac{\partial \psi_y}{\partial y} \right) + B_{12} \frac{\partial \delta \psi_x}{\partial x} + B_{22} \frac{\partial \delta \psi_y}{\partial y} \end{aligned} \right) \frac{\partial^2 w}{\partial y^2} \\ & + 2 * \left(\begin{aligned} & A_{66} \left(\frac{\partial \delta u_0}{\partial y} + \frac{\partial \delta v_0}{\partial x} + \frac{\partial w_0}{\partial y} \frac{\partial \delta w_0}{\partial x} \right. \\ & \quad \left. + \frac{\partial \delta w_0}{\partial y} \frac{\partial w_0}{\partial x} + \frac{\partial \delta w_0}{\partial x} \frac{\partial \delta w_0}{\partial y} \right) \right) \frac{\partial^2 w}{\partial x \partial y} \\ & + B_{66} \left(\frac{\partial \delta \psi_x}{\partial y} + \frac{\partial \delta \psi_y}{\partial x} \right) \\ & \left(\begin{aligned} & A_{66} \left(\frac{\partial u_0}{\partial y} + \frac{\partial v_0}{\partial x} + \frac{\partial w_0}{\partial x} \frac{\partial w_0}{\partial y} \right) \\ & + B_{12} \left(\frac{\partial \psi_y}{\partial y} \right) + B_{66} \left(\frac{\partial \delta \psi_x}{\partial y} + \frac{\partial \delta \psi_y}{\partial x} \right) \right) \frac{\partial^2 w}{\partial x \partial y} \\ & + A_{66} \left(\frac{\partial \delta u_0}{\partial y} + \frac{\partial \delta v_0}{\partial x} + \frac{\partial w_0}{\partial y} \frac{\partial \delta w_0}{\partial x} \right. \\ & \quad \left. + \frac{\partial \delta w_0}{\partial y} \frac{\partial w_0}{\partial x} + \frac{\partial \delta w_0}{\partial x} \frac{\partial \delta w_0}{\partial y} \right) \\ & - K_w \delta w + K_s \left(\frac{\partial^2 \delta w_0}{\partial x^2} + \frac{\partial^2 \delta w_0}{\partial y^2} \right) = 0 \end{aligned} \right) \end{aligned}$$

$$\begin{aligned}
 & B_{11} \left(\frac{\partial^2 \delta u_0}{\partial x^2} + \frac{\partial^2 w_0}{\partial x^2} \frac{\partial \delta w_0}{\partial x} \right) + \\
 & B_{12} \left(\frac{\partial^2 \delta v_0}{\partial x \partial y} + \frac{\partial^2 w_0}{\partial x \partial y} \frac{\partial \delta w_0}{\partial y} \right) + \\
 & + B_{66} \left(\frac{\partial^2 \delta u_0}{\partial y^2} + \frac{\partial^2 \delta v_0}{\partial x \partial y} + \frac{\partial^2 \delta w_0}{\partial x \partial y} \frac{\partial w_0}{\partial y} \right) + \\
 & \left(\frac{\partial \delta w_0}{\partial x} \frac{\partial^2 \delta w_0}{\partial y^2} + \frac{\partial^2 w_0}{\partial x \partial y} \frac{\partial \delta w_0}{\partial y} \right) + \\
 & \left(\frac{\partial w_0}{\partial x} \frac{\partial^2 \delta w_0}{\partial y^2} + \frac{\partial^2 \delta w_0}{\partial x \partial y} \frac{\partial \delta w_0}{\partial y} \right) + \\
 & \left(\frac{\partial \delta w_0}{\partial x} \frac{\partial^2 \delta w_0}{\partial y^2} \right) \\
 & + D_{11} \frac{\partial^2 \delta \psi_x}{\partial x^2} + D_{12} \frac{\partial^2 \delta \psi_y}{\partial x \partial y} + D_{66} \left(\frac{\partial^2 \delta \psi_x}{\partial y^2} + \frac{\partial^2 \delta \psi_y}{\partial x \partial y} \right) = 0 \\
 & B_{12} \left(\frac{\partial^2 \delta u_0}{\partial x \partial y} + \frac{\partial^2 w_0}{\partial x \partial y} \frac{\partial \delta w_0}{\partial x} \right) + \\
 & \left(\frac{\partial w_0}{\partial x} \frac{\partial^2 \delta w_0}{\partial x \partial y} + \frac{\partial \delta w_0}{\partial x} \frac{\partial^2 \delta w_0}{\partial x \partial y} \right) \\
 & + B_{22} \left(\frac{\partial^2 \delta v_0}{\partial y^2} + \frac{\partial^2 w_0}{\partial y^2} \frac{\partial \delta w_0}{\partial y} \right) + \\
 & \left(\frac{\partial w_0}{\partial y} \frac{\partial^2 \delta w_0}{\partial y^2} + \frac{\partial \delta w_0}{\partial y} \frac{\partial^2 \delta w_0}{\partial y^2} \right) \\
 & + B_{66} \left(\frac{\partial^2 \delta u_0}{\partial x \partial y} + \frac{\partial^2 \delta v_0}{\partial x^2} + \frac{\partial^2 \delta w_0}{\partial x^2} \frac{\partial w_0}{\partial y} \right) + \\
 & \left(\frac{\partial \delta w_0}{\partial x} \frac{\partial^2 \delta w_0}{\partial x \partial y} + \frac{\partial^2 w_0}{\partial x^2} \frac{\partial \delta w_0}{\partial y} \right) + \\
 & \left(\frac{\partial w_0}{\partial x} \frac{\partial^2 \delta w_0}{\partial x \partial y} + \frac{\partial^2 \delta w_0}{\partial x^2} \frac{\partial \delta w_0}{\partial y} \right) + \\
 & \left(\frac{\partial \delta w_0}{\partial x} \frac{\partial^2 \delta w_0}{\partial x \partial y} \right) \\
 & + D_{22} \frac{\partial^2 \delta \psi_y}{\partial y^2} + D_{12} \frac{\partial^2 \delta \psi_x}{\partial x \partial y} + D_{66} \left(\frac{\partial^2 \delta \psi_x}{\partial x \partial y} + \frac{\partial^2 \delta \psi_y}{\partial x^2} \right) = 0
 \end{aligned} \tag{21}$$

2.4. Boundary Conditions

For the buckling of CNTRC plates, the following boundary conditions are employed:

A-Clamped Support at $(x = 0, a)$ and $(y = 0, b)$

$$\begin{aligned}
 w = v = \psi_x = \psi_y = 0, \quad \delta N_x = -q \\
 w = u = \psi_x = \psi_y = 0, \quad \delta N_y = \pm q
 \end{aligned} \tag{22}$$

B-Simply Support at $(x = 0, a)$ and $(y = 0, b)$

$$\begin{aligned}
 w = v = \psi_y = \delta M_x = 0, \quad \delta N_x = -q \\
 w = u = \psi_x = \delta M_y = 0, \quad \delta N_y = \pm q
 \end{aligned} \tag{23}$$

3. Solution Method

Because of the effectiveness and efficiency of dynamic relaxation (DR) method to solve highly nonlinear problems, the DR technique in conjunction with finite difference discretization scheme has been employed in this study to analyze the nonlinear differential equations of the CNTRC plate. The DR is an explicit iterative procedure which is employed to transfer a boundary value problem into time-stepping initial value problem. This aim can be achieved by adding fictitious inertia and damping terms to the equilibrium equations (for more details see [26-27]):

$$[M]^n \{\ddot{X}\}^n + [C]^n \{\dot{X}\}^n + [K]^n \{X\}^n = \{F(t)\}^n \tag{24}$$

Where $[M]^n$, $[C]^n$ are fictitious mass and damping matrices, respectively. Also, $\{\dot{X}\}^n$, $\{\ddot{X}\}^n$ and $\{F(t)\}^n$ refer to vectors of virtual speed, acceleration and external forces at n^{th} iteration, respectively. In addition, $\{X\} = \{u, v, w, \psi_x, \psi_y\}$ is displacement vector and $[K]^n$ denotes stiffness matrix. Dynamic relaxation iteration method is generally unstable. So, the mass and damping matrices should be defined to guarantee the stability and convergence of the iterative procedure. In order to obtain explicit solution, matrix should be diametrical. Based on Gershgorin theorem, mass matrix is obtained through following expressions [27].

$$m_{ii} \geq \frac{1}{4} \Delta t^2 \sum_{j=1}^n |K_{ij}| \tag{25}$$

$$K = \frac{\partial P}{\partial X} \tag{26}$$

In above expressions, P_i is internal forces (the left-hand side of the equilibrium equations (Eqs. (21)). Based on Zhang's suggestion, the damping coefficient can be determined according to the following expression [27]:

$$c_n = 2 \left\{ \frac{\{X_n\}^T \{F(X_n)\}}{\{X_n\}^T [M_n] \{X_n\}} \right\}^{\frac{1}{2}} \tag{27}$$

In addition, damping matrix should be dependent to the mass matrix according to the following expression:

$$[C] = c[M] \tag{28}$$

To complete the transformation process, the velocity and acceleration terms must be replaced with the following equivalent central finite-difference expressions:

$$\{\ddot{X}\}^n = \frac{\{\dot{X}\}^{n+\frac{1}{2}} - \{\dot{X}\}^{n-\frac{1}{2}}}{\Delta t} \tag{29}$$

$$\{\dot{X}\}^{n-\frac{1}{2}} = \frac{\{X\}^n - \{X\}^{n-1}}{\Delta t} \quad (30)$$

By substituting Eqs. (29) and (30) in Eq. (24), the equilibrium equations can be rearranged into an initial value format as follows:

$$\dot{u}_i^{n+\frac{1}{2}} = \frac{2\Delta t^n}{2+c_i^n\Delta t^n} (m_{ii}^n)^{-1} \left(\frac{\partial \delta N_{xx}}{\partial x} + \frac{\partial \delta N_{xy}}{\partial y} \right)_i + \frac{2-c_i^n\Delta t^n}{2+c_i^n\Delta t^n} \dot{u}_i^{n-\frac{1}{2}}$$

$$\dot{v}_i^{n+\frac{1}{2}} = \frac{2\Delta t^n}{2+c_i^n\Delta t^n} (m_{ii}^n)^{-1} \left(\frac{\partial \delta N_{xy}}{\partial x} + \frac{\partial \delta N_{yy}}{\partial y} \right)_i + \frac{2-c_i^n\Delta t^n}{2+c_i^n\Delta t^n} \dot{v}_i^{n-\frac{1}{2}}$$

$$\dot{w}_i^{n+\frac{1}{2}} = \frac{2\Delta t^n}{2+c_i^n\Delta t^n} (m_{ii}^n)^{-1} \left(\begin{aligned} &\frac{\partial \delta Q_x}{\partial x} + \frac{\partial \delta Q_y}{\partial y} \\ &+\delta N_{xx} \left(\frac{\partial^2 w}{\partial x^2} \right) \\ &+\delta N_{yy} \left(\frac{\partial^2 w}{\partial y^2} \right) \\ &+2\delta N_{xy} \left(\frac{\partial^2 w}{\partial x \partial y} \right) \\ &+(N_{xx} + \delta N_{xx}) \frac{\partial^2 \delta w}{\partial x^2} \\ &+(N_{yy} + \delta N_{yy}) \frac{\partial^2 \delta w}{\partial y^2} \\ &+2(N_{xy} + \delta N_{xy}) \frac{\partial^2 \delta w}{\partial x \partial y} \end{aligned} \right)$$

$$+ \frac{2-c_i^n\Delta t^n}{2+c_i^n\Delta t^n} \dot{w}_i^{n-\frac{1}{2}}$$

$$(\dot{\psi}_x)_i^{n+\frac{1}{2}} = \frac{2\Delta t^n}{2+c_i^n\Delta t^n} (m_{ii}^n)^{-1} \left(\frac{\partial \delta M_{xx}}{\partial x} + \frac{\partial \delta M_{xy}}{\partial y} - \delta Q_x \right)_i + \frac{2-c_i^n\Delta t^n}{2+c_i^n\Delta t^n} (\dot{\psi}_x)_i^{n-\frac{1}{2}}$$

$$(\dot{\psi}_y)_i^{n+\frac{1}{2}} = \frac{2\Delta t^n}{2+c_i^n\Delta t^n} (m_{ii}^n)^{-1} \left(\frac{\partial \delta M_{xy}}{\partial x} + \frac{\partial \delta M_{yy}}{\partial y} - \delta Q_y \right)_i + \frac{2-c_i^n\Delta t^n}{2+c_i^n\Delta t^n} (\dot{\psi}_y)_i^{n-\frac{1}{2}}$$

(31)

By integrating the velocities at the end of each load step, the incremental displacements can be obtained as:

$$\{\delta X\}^{n+1} = \{\delta X\}^n + \Delta t \{\delta \dot{X}\}^{n+\frac{1}{2}} \quad (32)$$

Therefore, the displacement equilibrium equations and Eqs. (31)-(32) together with the appropriate boundary conditions in their finite difference forms, constitute the set of equations for the sequential DR method. For the sake of

brevity, the DR algorithm which is clearly explained in [26, 27] is omitted.

In order to find the critical buckling load from the load-displacement curve the total displacements of each load must be computed. For this purpose, the obtained incremental displacements in each load step should be added to the displacements determined from the previous load steps as follows:

$$\{X\}^n = \{X\}^{n-1} + \{\delta X\}^n \quad (33)$$

This process continues till the code diverges, and this is a sign of buckling event. Clearly, critical buckling load is a specified load in which a large amount of displacement is occurred compared to the previous load steps.

4. Results and Discussion

4.1. Material Comparison study

In Table 1, the present solutions for buckling loads of CNTRC plates with clamped and simply supported boundary conditions and different arrangements of CNTs and loadings are compared with the results reported by Lei et al. [28]. It is noted that loadings include uniaxial compression along axis x ($\gamma_1 = -1, \gamma_2 = 0$), biaxial compression ($\gamma_1 = -1, \gamma_2 = -1$) and biaxial compressive and tensile loading ($\gamma_1 = -1, \gamma_2 = 1$). As shown in Table 1, for different load conditions, the current solutions are in good consistency with those of Lei et al. [28] and the reliability and accuracy of the present formulation and results are verified.

4.2. Parametric Study

In this section, the effects of various parameters on the buckling behavior of FG-CNTRC plate are presented. The material properties of polymeric phase are taken from [16]. Also, the elastic properties of SWCNTs in armchair state (10 and 10) are considered as $E_{11} = 5.6466(\text{TPa})$, $E_{22} = 5.0800(\text{TPa})$, $G_{12} = 1.9445(\text{TPa})$ which are reported in [19].

Table 2 shows the Young modulus of CNTRC plate in x and y directions as well as CNT efficiency parameters $\eta_j (j=1,2,3)$ which are taken from [5, 19] based on MD and modified rule of mixture, respectively, for various values of CNTs volume fractions. Furthermore, as reported by Shen and Zhang [19], $G_{13} = G_{12}$, $G_{23} = 1.2G_{12}$ and $\eta_3 = 0.7\eta_2$.

In the following results, the effects of nanotubes volume fraction, distribution of nanotubes, width-to-thickness ratio of plates and plate geometry are investigated on the critical buckling load of nanocomposite plates with

clamped and simply supported boundary conditions. In the results, the boundary conditions are considered with all edges clamped and simply supported which named by CCCC and SSSS, respectively. The dimensionless buckling load is defined by $P = N_{cr} b^2 / E_m h^3$ and the plate thickness is assumed with $h = 2mm$.

Fig. 2 and Fig. 3 show the dimensionless buckling load of simply supported nanocomposite plate in terms of volume fractions of CNTs for different distributions of CNTs, loading states and two width-to-thickness ratios $b/h=50$ and $b/h=10$, respectively. As seen, the FG-X and FG-O distributions have the highest and lowest values of buckling loads, respectively, for all loading states, CNTs distributions and width-to-thickness ratios. Furthermore, increase of CNTs volume fraction from 0.12 to 0.17 causes a significant rise of buckling load for different CNTs distributions and loading states. While, increasing the CNTs volume fraction from 0.17 to 0.28 does not have significant effect on the buckling load.

Considering the results for two different width-to-thickness ratios of $b/h=50$ and $b/h=10$ shows that increasing CNTs volume fraction has the greater effect on the buckling strength of nanocomposite plate. Also, it is seen that increasing the thickness of nanocomposite plate has the more effect on the buckling load for FG distribution of CNTs compared to uniform ones.

Table 1 Comparison of dimensionless buckling load $N_x = N_{cr} b^2 / E_m h^3$ between the present study and those of Lei [28] for different boundary conditions, loading and CNTs distribution.

		Present study	Lei [28]	Present study	Lei [28]
		C	C	SS	SS
$\gamma_1 = -1, \gamma_2 = 0$	UD	25.19	25.73	13.75	14.11
	FG-X	26.67	27.89	16.15	17.06
	FG-O	22.38	21.12	10.55	9.83
	FG-V	24.54	-	13.43	-
$\gamma_1 = -1, \gamma_2 = 1$	UD	30.95	31.10	27.82	28.47
	FG-X	31.43	31.39	28.98	29.18
	FG-O	27.14	27.93	25.26	24.05
	FG-V	31.43	-	28.98	-
$\gamma_1, \gamma_2 = -1$	UD	9.0476	9.28	5.71	5.88
	FG-X	9.54	9.65	6.19	6.44
	FG-O	8.57	8.60	5.00	4.90
	FG-V	8.57	-	5.00	-

Table 2 Young's moduli for PMMA/CNT composites reinforced by (10, 10) tube in room temperature reported by [5] and [19].

V_{CNT}^*	MD (Ref. [5])		Rule of mixture [19]			
	E_{11}	E_{22}	E_{11}	η_1	E_{22}	η_2
0.12	94.6	2.9	94.78	0.137	2.9	1.022
0.17	138.9	4.9	138.68	0.142	4.9	1.626
0.28	224.2	5.5	224.5	0.141	5.5	1.585

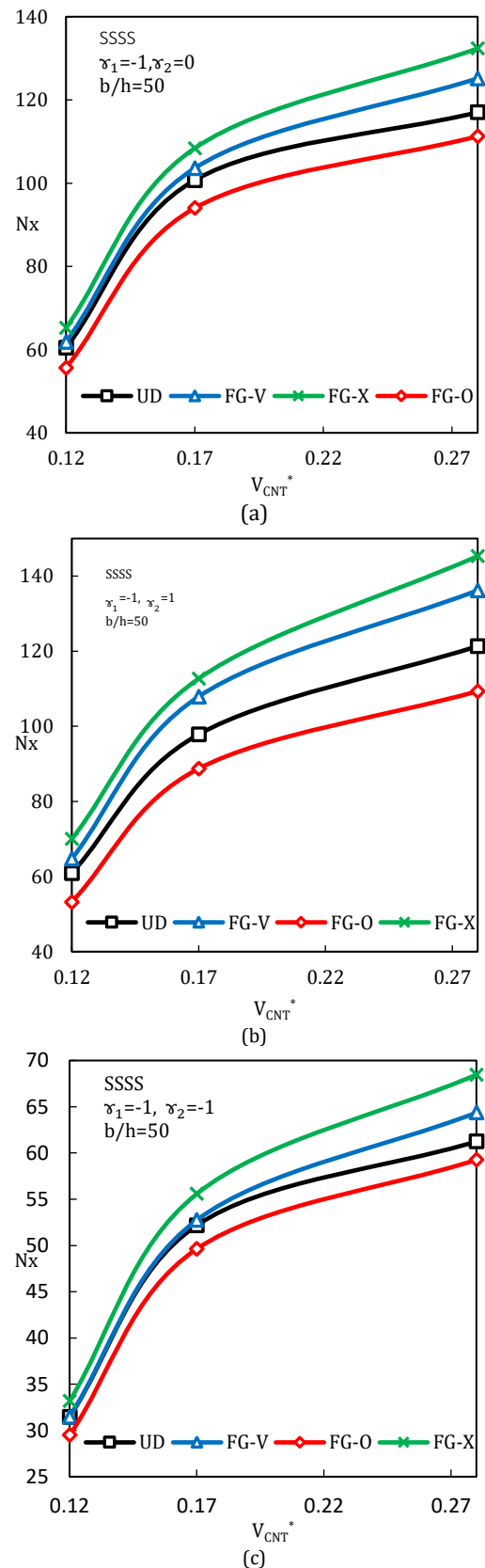


Fig. 2 Effect of CNTs volume fraction on the buckling load of FG-CNTRC plate ($b/h=50$) with simply supported boundary conditions for (a) $(\gamma_1 = -1, \gamma_2 = 0)$, (b) $(\gamma_1 = -1, \gamma_2 = 1)$ and (c) $(\gamma_1 = -1, \gamma_2 = -1)$.

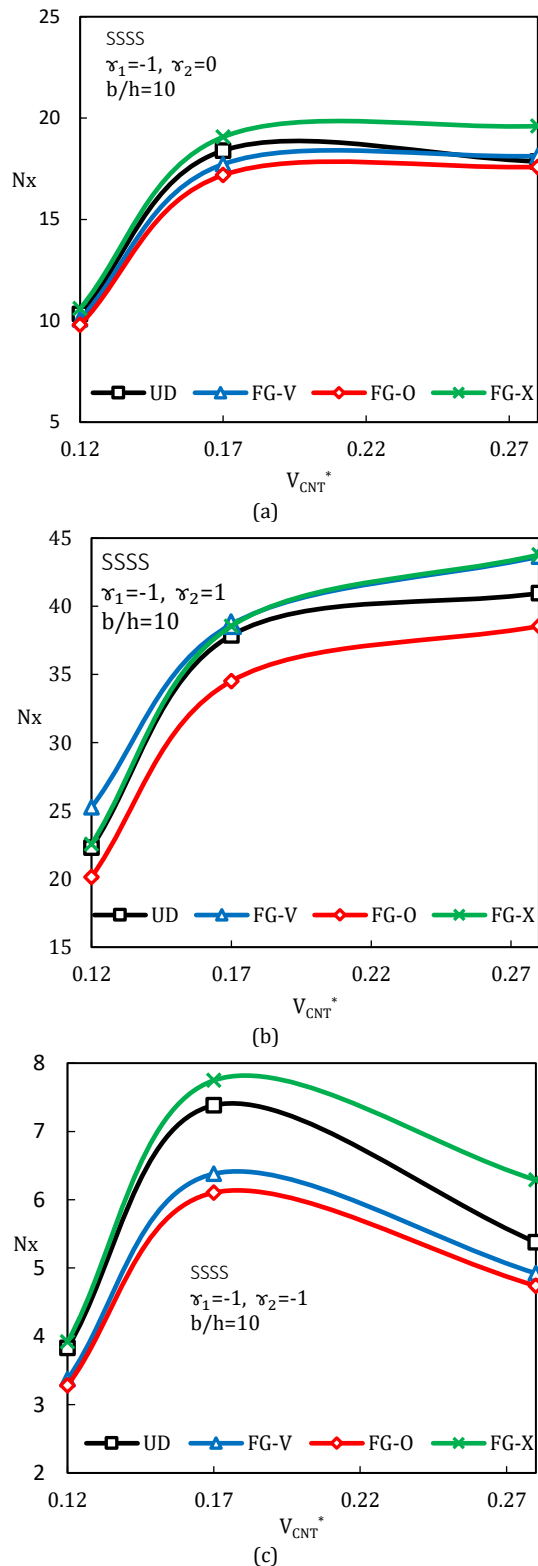


Fig. 3 Effect of CNTs volume fraction on the buckling load of FG-CNTRC plate ($b/h=10$) with simply supported boundary conditions for (a) $(\gamma_1=-1, \gamma_2=0)$, (b) $(\gamma_1=-1, \gamma_2=1)$ and (c) $(\gamma_1=-1, \gamma_2=-1)$.

Fig. 4 and Fig. 5 consider the effect of width-to-length ratio of FG-CNTRC plate ($V_{CNT}^*=0.17$ and $b/h=20$) on the buckling load with different loading types for clamped and simply supported

boundary conditions, respectively. As seen, for two loading modes of $(\gamma_1=-1, \gamma_2=0)$ and $(\gamma_1=-1, \gamma_2=1)$ the buckling load decreases by increasing the width-to-length ratio in both CCCC and SSSS boundary conditions. Furthermore, the decrease of buckling load is more significant for biaxial compressive-tensile load $(\gamma_1=-1, \gamma_2=1)$ compared to uniaxial compressive load $(\gamma_1=-1, \gamma_2=0)$. Furthermore, it is depicted that effect of width-to-length ratio on the buckling load of CCCC boundary condition is much less than the SSSS one (50% decrease versus 30% decrease by 2.5 times increase of width-to-length ratio for different CNTs distributions). However, for loading type of $(\gamma_1=-1, \gamma_2=0)$, highest and lowest decline of dimensionless buckling load are associated with FG-O (i.e., 42 percent) and FG-X (i.e., 21 percent) distributions, respectively. It can be rephrased that FG-X distribution has the highest buckling resistance against reduction of critical buckling load for both of loading modes. Finally, as shown in Fig. 4 (c) in the case of biaxial compressive loading $(\gamma_1=-1, \gamma_2=-1)$ and clamped boundary condition, by raising the width-to-length ratio the variation of buckling load be completely different compared to other loading types. For example, in clamped boundary condition and loading type of biaxial compression increasing the width-to-length ratio to a specified value goes up the buckling load significantly and more increase of this ratio does not have considerable effect on the buckling load.

However, as illustrated in Fig. 5 (c), for SSSS boundary condition and UD, FG-X and FG-V distributions with growing up the width-to-length ratio a little increase of buckling load can be observed. Although, in SSSS case and FG-O distribution increasing this ratio decreases the buckling load smoothly.

In the following results, the buckling behavior of CNT reinforced composite plate on elastic foundation has been studied for different volume fraction of CNTs, width-to-thickness ratios, width-to-length ratios and two types of CCCC and SSSS boundary conditions.

Tables 3 to 5 show the effects of elastic foundation coefficient (K_w, K_s) on dimensionless buckling load of nanocomposite plate with thickness of $h=2mm$, the width-to-thickness ratio ($b/h=10$) and volume fraction ($V_{CNT}^*=0.17$) with SSSS and CCCC boundary conditions for uniaxial compressive loading $(\gamma_1=-1, \gamma_2=0)$, compressive-tensile loading $(\gamma_1=-1, \gamma_2=1)$ and biaxial compressive loading $(\gamma_1=-1, \gamma_2=-1)$, respectively.

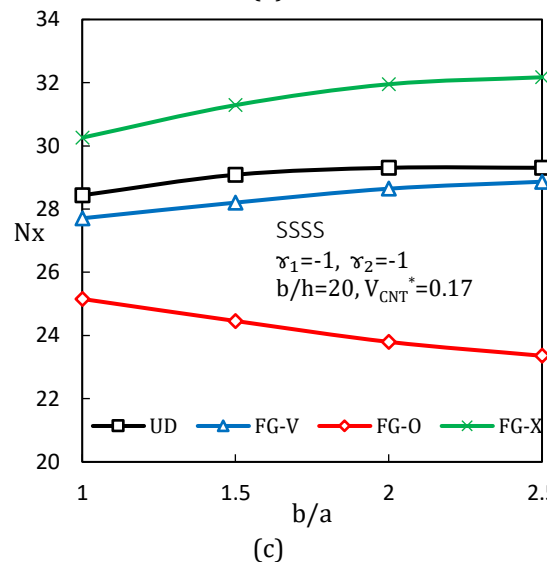
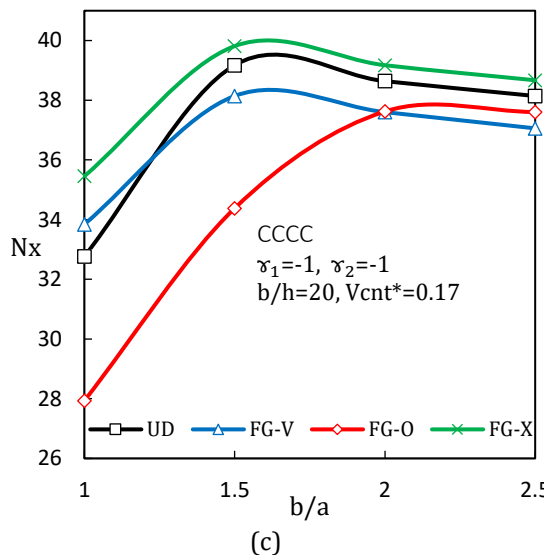
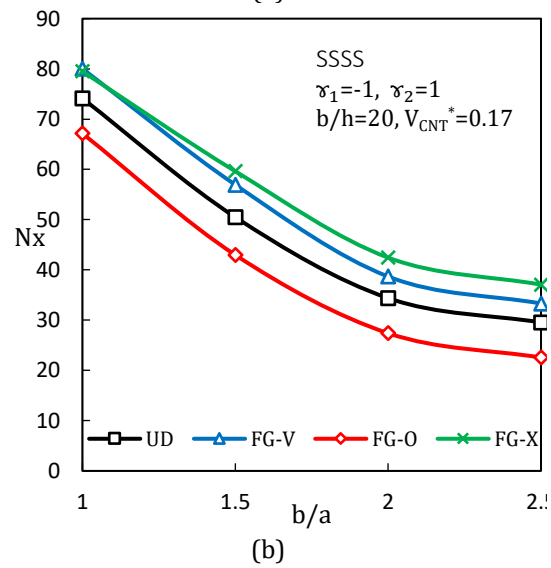
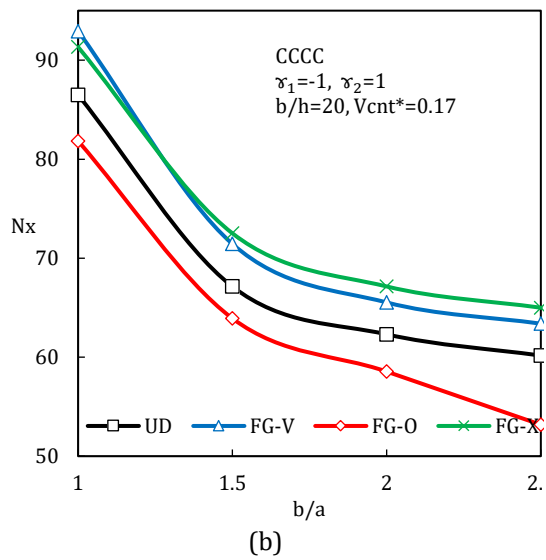
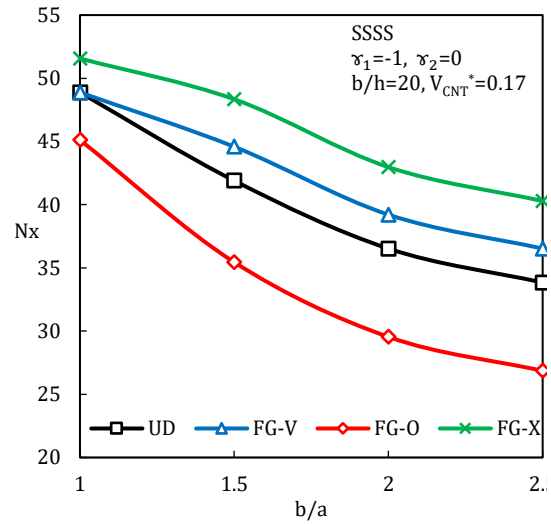
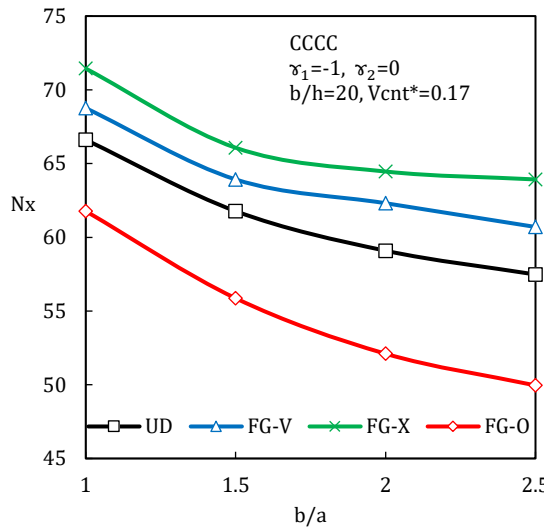


Fig. 4 Effect of width-to-length ratio on the buckling load of FG-CNTRC plate ($b/h = 20, V_{CNT}^* = 0.17$) with clamped boundary conditions for (a) ($\gamma_1 = -1, \gamma_2 = 0$), (b) ($\gamma_1 = -1, \gamma_2 = 1$) and (c) ($\gamma_1 = -1, \gamma_2 = -1$).

Fig. 5 Effect of width-to-length ratio on the buckling load of FG-CNTRC plate ($b/h = 20, V_{CNT}^* = 0.17$) with simply supported boundary conditions for (a) ($\gamma_1 = -1, \gamma_2 = 0$), (b) ($\gamma_1 = -1, \gamma_2 = 1$) and (c) ($\gamma_1 = -1, \gamma_2 = -1$).

Table 3 Effects of Elastic Substrate (K_s and K_w) on Dimensionless Buckling Load of Nanocomposite Plate ($(h=2mm)$, $(b/h=10)$ and $(V_{CNT}^*=0.17)$) and uniaxial compressive load ($\gamma_1=-1, \gamma_2=0$).

K_w	K_s	UD	FG-V	FG-X	FG-O
		Simply Support			
0	0	18.40	17.73	19.07	17.19
	20	18.67	17.99	19.34	17.46
	50	19.07	18.4	19.74	17.76
20	0	20.01	19.20	20.55	18.80
	20	20.28	19.47	20.81	19.07
	50	20.68	19.87	21.22	19.47
50	0	22.29	21.49	22.83	21.08
	20	22.56	21.75	23.10	21.35
	50	22.96	22.16	23.50	21.75
Clamped Support					
0	0	34.11	34.38	35.05	31.42
	20	34.51	34.78	35.59	31.83
	50	35.05	35.45	36.12	32.36
20	0	36.39	36.53	37.33	32.77
	20	36.93	36.93	37.60	33.17
	50	37.33	37.60	38.27	33.71
50	0	39.21	39.48	30.02	34.51
	20	39.61	39.75	40.42	34.78
	50	40.15	40.42	40.96	35.32

Table 4 Effects of Elastic Substrate (K_s and K_w) on Dimensionless Buckling Load of Nanocomposite Plate ($(h=2mm)$, $(b/h=10)$ and $(V_{CNT}^*=0.17)$) and biaxial compressive-tensile load ($\gamma_1=-1, \gamma_2=1$).

K_w	K_s	UD	FG-V	FG-X	FG-O
		Simply Support			
0	0	37.8704	38.6761	38.5418	34.5131
	20	38.2732	39.079	38.9447	34.7816
	50	38.8104	39.7504	39.6161	35.4531
20	0	38.8104	39.7504	39.4818	35.1845
	20	39.2133	40.1533	39.8847	35.5874
	50	39.7504	40.6905	40.5562	36.1245
50	0	40.1533	41.0934	40.8248	36.1245
	20	40.4219	41.4962	41.2276	36.3931
	50	41.0934	42.0334	41.7648	37.0646
Clamped Support					
0	0	42.302	43.6449	43.2421	37.796
	20	42.7049	44.0478	42.6449	37.1989
	50	43.5106	44.7192	44.3164	37.7361
20	0	43.9135	45.2564	44.8535	37.7361
	20	44.364	45.6593	45.2564	38.1389
	50	44.9878	46.3307	45.9279	38.6761
50	0	46.1965	47.5394	47.0022	39.2133
	20	46.5993	48.0765	47.5394	39.6161
	50	47.2708	48.748	48.765	40.1533

For all types of loading, CNTs distributions and boundary conditions the effect of Winkler coefficient on increase of critical dimensionless buckling load is significantly higher than shear coefficient of the substrate (K_s). As seen, for all types of loading and both cases of with and without presence of elastic foundation the FG-X and FG-O have the highest and lowest values of

buckling loads, respectively, for both SSSS and CCCC boundary conditions.

Fig. 6 represent the effect of CNTs volume fraction on the critical buckling load of SSSS nano-composite plate with UD and FG distributions for different coefficients of elastic substrate (K_w, K_s) and various types of loadings.

As seen, for both types of UD and FG distributions of nano-composite plate with and without presence of elastic foundation increasing the volume fraction of CNTs from 0.12 to 0.17 causes a significant increase of buckling load. However, by increasing the volume fraction of CNTs from 0.17 to 0.28 the raising rate of buckling load decreases for both types of with and without elastic foundation and CNTs distributions. Obviously, presence of elastic foundation increases the buckling load and the effect of Winkler foundation on the buckling load is much greater than the shear coefficient of Pasternak foundation.

Fig. 7 show the effect of width-to-thickness ratio on the buckling load of SSSS nano-composite plate with and without elastic foundation and two types of UD and FG-X distributions for loading types of (a) ($\gamma_1=-1, \gamma_2=0$), (b) ($\gamma_1=-1, \gamma_2=1$) and (c) ($\gamma_1=-1, \gamma_2=-1$). As seen, with increase of width-to-thickness ratio the influence of elastic foundation on the buckling load goes up significantly. Furthermore, the effect of CNTs distribution on the buckling load is much greater when the elastic foundation does not exist.

Table 5 Effects of Elastic Substrate (K_s and K_w) on Dimensionless Buckling Load of Nanocomposite Plate ($(h=2mm)$, $(b/h=10)$ and $(V_{CNT}^*=0.17)$) and biaxial compressive load ($\gamma_1=-1, \gamma_2=-1$).

K_w	K_s	UD	FG-V	FG-X	FG-O
		Simply Support			
0	0	7.3266	6.3801	7.7473	6.1038
	20	7.4919	6.4573	7.8449	6.1905
	50	7.7122	6.6708	8.0583	6.4040
20	0	8.2080	7.0977	8.592	6.8843
	20	8.3733	7.2578	8.6987	6.9910
	50	8.5936	7.4713	8.9656	7.2578
50	0	9.5526	8.3252	9.8728	8.1117
	20	9.7661	8.4319	10.0863	8.2184
	50	9.9262	8.6987	10.2997	8.4853
Clamped Support					
0	0	13.0263	12.0863	13.4292	11.9520
	20	13.2949	12.3549	13.6978	12.0863
	50	13.5635	12.6234	13.9664	12.3549
20	0	13.9664	12.892	14.3692	12.7579
	20	14.1007	13.1606	14.5035	12.8921
	50	14.3692	13.4292	14.9064	13.2949
50	0	15.1750	14.1007	15.5779	13.8321
	20	15.3093	14.2350	15.7122	14.1007
	50	15.5779	14.5035	16.1151	14.3692

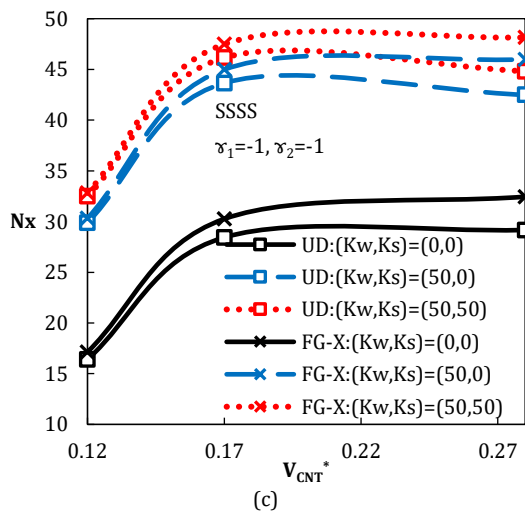
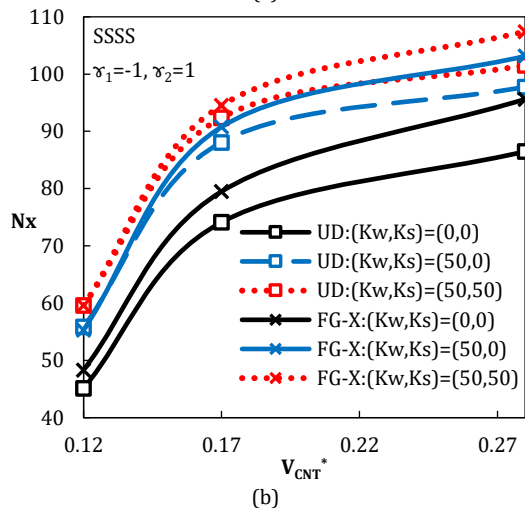
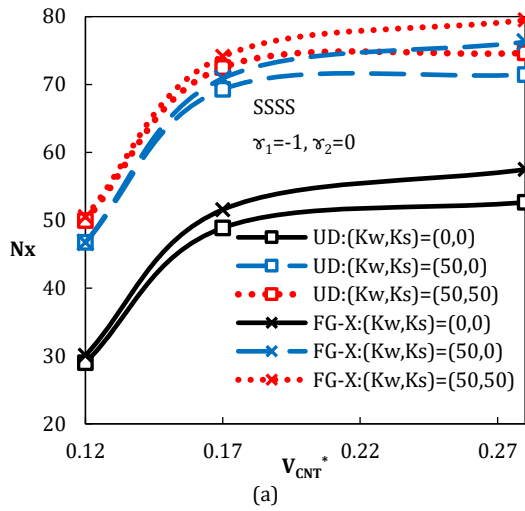


Fig. 6 Effect of CNTs volume fraction on the dimensionless buckling load of simply supported FG-CNTRC plate ($b/h = 20$) with different elastic foundation coefficients for (a) ($\gamma_1 = -1, \gamma_2 = 0$), (b) ($\gamma_1 = -1, \gamma_2 = 1$) and (c) ($\gamma_1 = -1, \gamma_2 = -1$).

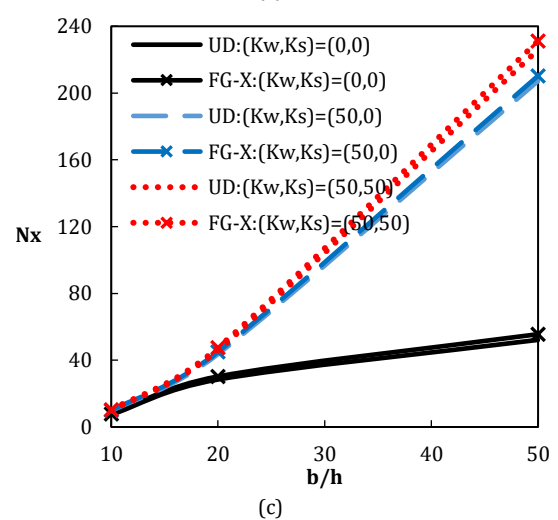
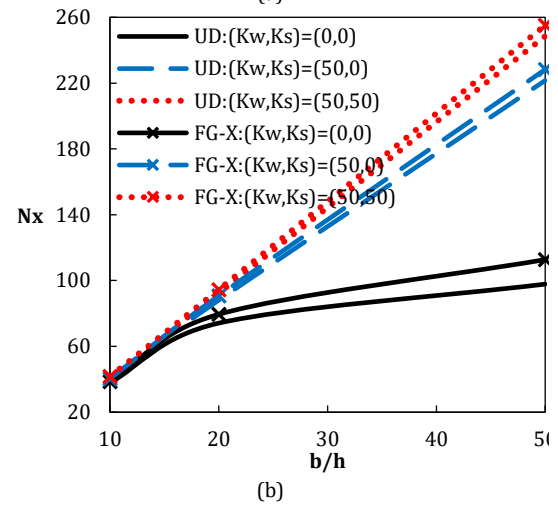
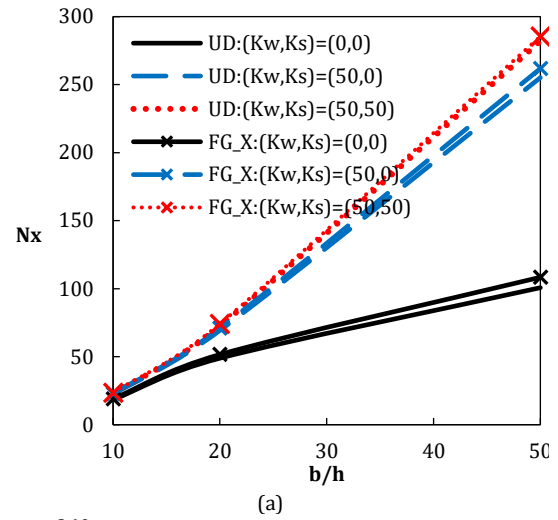


Fig. 7 Effect of width-to-thickness ratio on the dimensionless buckling load of simply supported FG-CNTRC plate ($V_{CNT}^* = 0.17$) with different elastic foundation coefficients for (a) ($\gamma_1 = -1, \gamma_2 = 0$), (b) ($\gamma_1 = -1, \gamma_2 = 1$) and (c) ($\gamma_1 = -1, \gamma_2 = -1$).

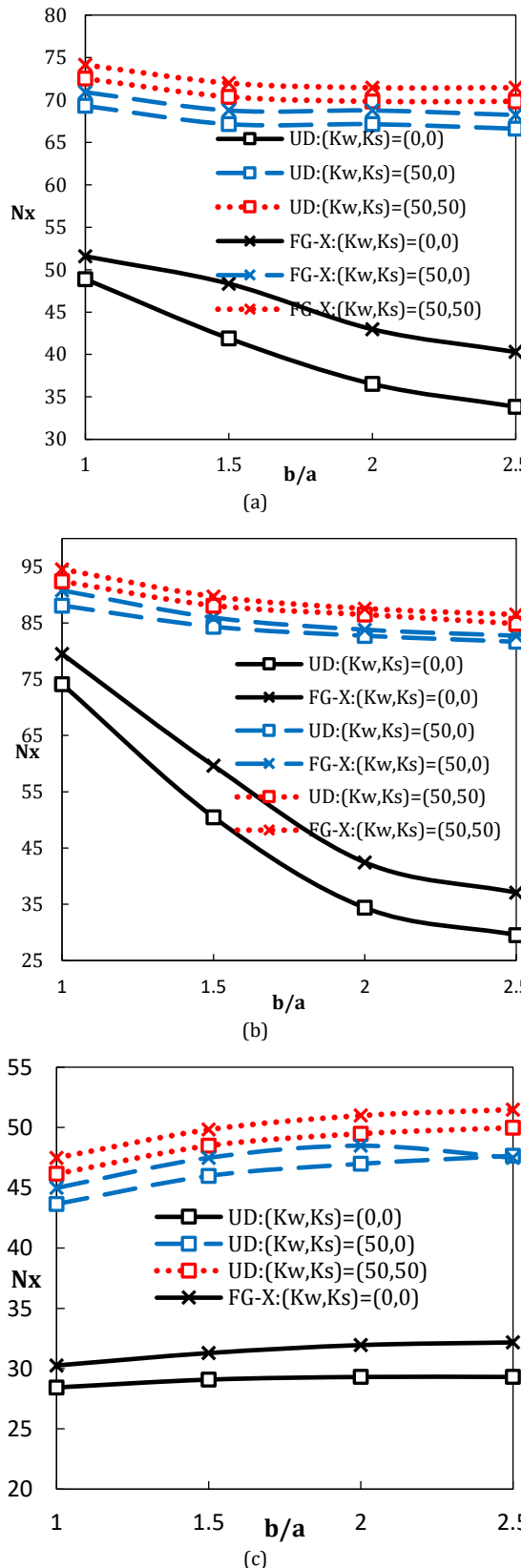


Fig. 8 Effect of width-to-length ratio on the dimensionless buckling load of simply supported FG-CNTRC plate ($b/h = 20, V_{CNT}^* = 0.17$) with different elastic foundation coefficients for (a) $(\gamma_1 = -1, \gamma_2 = 0)$, (b) $(\gamma_1 = -1, \gamma_2 = 1)$ and (c) $(\gamma_1 = -1, \gamma_2 = -1)$.

Fig. 8 illustrate the effect of width-to-length ratio on the buckling load of UD and FG-X nanocomposite plate with and without presence of elastic foundation for loading types of (a) $(\gamma_1 = -1, \gamma_2 = 0)$, (b) $(\gamma_1 = -1, \gamma_2 = 1)$ and (c) $(\gamma_1 = -1, \gamma_2 = -1)$. Obviously, with increase of aspect ratio the buckling load decreases for both loading types of uniaxial compressive load $(\gamma_1 = -1, \gamma_2 = 0)$ and compressive-tensile load $(\gamma_1 = -1, \gamma_2 = 1)$ and the decrease rate is greater in compressive-tensile loading compared to uniaxial compressive case. But, against the mentioned loading types, increase of aspect ratio raises the buckling load gradually. It is also observed that the effect of Winkler module on the buckling load is much greater than the shear elastic foundation.

5. Conclusions

Based on incremental load technique a new method is presented for buckling analysis of single-walled carbon nanotube reinforced composite plates resting on an elastic foundation and subjected to different tensile-compressive loads. A uniform and three kinds of functionally graded distributions of CNTs along the thickness direction of plate are considered.

The properties of composite material in each point were determined by modified rule of mixture. All governing equations were obtained incrementally based on first order shear deformation theory (FSTD) and Von Karman nonlinear strains. Using the principle of minimum potential energy, the set of coupled nonlinear equilibrium equations was obtained in incremental form for different boundary conditions. The dynamic relaxation (DR) method combined with the finite difference discretization technique is employed to find the critical buckling load for simply supported and clamped boundary conditions. Some major inferences are as follows:

It is seen that increasing the thickness of nanocomposite plate has the more effect on the buckling load for FG distribution of CNTs compared to uniform ones.

For all types of loading and both cases of with and without presence of elastic foundation the FG-X and FG-0 have the highest and lowest values of buckling loads, respectively, for both SSSS and CCCC boundary conditions.

For both types of with and without elastic foundation, CNTs distributions and boundary conditions, increasing the volume fraction of CNTs from 0.12 to 0.17 causes a significant increase of buckling load. However, by increasing the volume fraction of CNTs from 0.17 to 0.28 the raising rate of buckling load decreases.

Nomenclature

a, b, h	length, width and thickness of CNTRC plate
E_{11}, E_{22}, G_{12}	elasticity modulus and shear modulus of CNTRC plate
E_m, G_m	elasticity modulus and shear modulus of matrix
$E_{11}^{CNT}, E_{22}^{CNT}, G_{12}^{CNT}$	elasticity modulus and shear modulus of carbon nanotubes
V_m, V_{CNT}	volume fractions of substrate and carbon nanotubes
η_1, η_2, η_3	CNT efficiency parameters
w_{CNT}	mass fraction of carbon nanotubes in composite plate
ρ^m, ρ^{CNT}	densities of substrate and carbon nanotubes
$\nu_{12}, \nu^m, \nu_{12}^{CNT}$	Poisson's ratio of CNTRC plate, substrate and CNT
u, v, w	displacement components in x, y and z directions, respectively
u_0, v_0, w_0	displacement components of the mid-plane
ψ_x, ψ_y	rotations of transverse normal about y and x axes
$\delta \varepsilon_{ij}$	incremental strain components
$\delta \sigma_{ij}$	incremental stress components
Q_{ij}	Plane stress-reduced stiffnesses
$\delta N_{ij}, \delta M_{ij}$	incremental forces, moments and shear stress resultants
$\delta Q_y, \delta Q_x$	
$[A], [B], [D], [A^s]$	extensional, coupling, bending, and shear stiffness
k_s	transverse shear correction coefficient
K_w, K_s	Winkler and shear coefficients of foundation parameters

References

- [1] Thostenson, E. T., Ren, Z., Chou, T.-W., 2001. Advances in the science and technology of carbon nanotubes and their composites: a review. *Composites Science and Technology*, 61(13), pp.1899-1912
- [2] Fiedler, B., Gojny, F. H., Wichmann, M. H., Nolte, M. C., Schulte, K., 2006. Fundamental aspects of nano-reinforced composites. *Composites Science and Technology*, 66(16), pp.3115-3125.
- [3] Fidelus, J., Wiesel, E., Gojny, F., Schulte, K., Wagner, H., 2005. Thermo-mechanical properties of randomly oriented carbon/epoxy nanocomposites. *Composites Part A: Applied Science and Manufacturing*, 36(11), pp.1555-1561.
- [4] Anumandla, V., Gibson, R. F., 2006. A comprehensive closed form micromechanics model for estimating the elastic modulus of nanotube-reinforced composites. *Composites Part A: Applied Science and Manufacturing*, 37(12), pp.2178-2185.
- [5] Han, Y., Elliott, J., 2007. Molecular dynamics simulations of the elastic properties of polymer/carbon nanotube composites. *Computational Materials Science*, 39(2), pp.315-323.
- [6] Cooper, C. A., Cohen, S. R., Barber, A. H., Wagner, H. D., 2002. Detachment of nanotubes from a polymer matrix. *Applied Physics Letters*, 81(20), pp.3873-3875.
- [7] Barber, A. H., Cohen, S. R., Wagner, H. D., 2003. Measurement of carbon nanotube-polymer interfacial strength. *Applied Physics Letters*, 82(23), pp.4140-4142.
- [8] Gou, J., Minaie, B., Wang, B., Liang, Z., Zhang, C., 2004. Computational and experimental study of interfacial bonding of single-walled nanotube reinforced composites. *Computational Materials Science*, 31(3-4), pp.225-236.
- [9] Frankland, S., Caglar, A., Brenner, D., Griebel, M., 2002. Molecular simulation of the influence of chemical cross-links on the shear strength of carbon nanotube-polymer interfaces. *The Journal of Physical Chemistry B*, 106(12), pp.3046-3048.
- [10] Ma, P.-C., Mo, S.-Y., Tang, B.-Z., Kim, J.-K., 2010. Dispersion, interfacial interaction and re-agglomeration of functionalized carbon nanotubes in epoxy composites. *Carbon*, 48(6), pp.1824-1834.
- [11] Coleman, J. N., Khan, U., Blau, W. J., Gun'ko, Y. K., 2006. Small but strong: a review of the mechanical properties of carbon nanotube-polymer composites. *Carbon*, 44(9), pp.1624-1652.
- [12] Wuite, J., Adali, S., 2005. Deflection and stress behaviour of nanocomposite reinforced beams using a multiscale analysis. *Composite Structures*, 71(3-4), pp.388-396.
- [13] Vodenitcharova, T., Zhang, L., 2006. Bending and local buckling of a nanocomposite beam reinforced by a single-walled carbon nanotube. *International journal of solids and structures*, 43(10), pp.3006-3024.
- [14] Formica, G., Lacarbonara, W., Alessi, R., 2010. Vibrations of carbon nanotube-reinforced composites. *Journal of Sound and Vibration*, 329(10), pp.1875-1889.

- [15] Arani, A. G., Maghamikia, S., Mohammadimehr, M., Arefmanesh, A., 2011. Buckling analysis of laminated composite rectangular plates reinforced by SWCNTs using analytical and finite element methods. *Journal of Mechanical Science and Technology*, 25(3), pp.809-820.
- [16] Shen, H.S., 2009. Nonlinear bending of functionally graded carbon nanotube-reinforced composite plates in thermal environments. *Composite Structures*, 91(1), pp.9-19.
- [17] Zhu, P., Lei, Z., Liew, K. M., 2012. Static and free vibration analyses of carbon nanotube-reinforced composite plates using finite element method with first order shear deformation plate theory. *Composite Structures*, 94(4), pp.1450-1460.
- [18] Ke, L.L., Yang, J., Kitipornchai, S., 2010. Nonlinear free vibration of functionally graded carbon nanotube-reinforced composite beams. *Composite Structures*, 92(3), pp.676-683.
- [19] Shen, H.S., Zhang, C.L., 2010. Thermal buckling and postbuckling behavior of functionally graded carbon nanotube-reinforced composite plates. *Materials and Design*, 31(7), pp.3403-3411.
- [20] Mohammadi, M., Arefi, M., Dimitri, R., Tornabene, F., 2019. Higher-order thermo-elastic analysis of FG-CNTRC cylindrical vessels surrounded by a Pasternak foundation. *Nanomaterials*, 9(1), 79.
- [21] Mohammadi, M., Arefi, M., Ahmadi, S. A., 2020. Two-dimensional electro-elastic analysis of FG-CNTRC cylindrical laminated pressure vessels with piezoelectric layers based on third-order shear deformation theory. *Journal of Pressure Vessel Technology*, 142(2), 021304.
- [22] Wang, Z.X., Shen, H.S., 2011. Nonlinear vibration of nanotube-reinforced composite plates in thermal environments. *Computational Materials Science*, 50(8), pp.2319-2330.
- [23] Arefi, M., Mohammadi, M., Rabczuk, T., 2019. Effect of characteristics and distribution of porosity on electro-elastic analysis of laminated vessels with piezoelectric face-sheets based on higher-order modeling. *Composite Structures*, 225, 111085.
- [24] Reddy, J. N., 2004. *Mechanics of laminated composite plates and shells: theory and analysis*. CRC press.
- [25] Kadkhodayan, M., Zhang, L., Sowerby, R., 1997. Analyses of wrinkling and buckling of elastic plates by DXDR method. *Computers and Structures*, 65(4), pp.561-574.
- [26] Zhang, L., Kadkhodayan, M., Mai, Y.-W., 1994. Development of the maDR method. *Computers and Structures*, 52(1), pp.1-8.
- [27] Underwood, P., 1983. Dynamic relaxation in computational method for transient analysis. *Amsterdam: Elsevier*, 245-265.
- [28] Lei, Z., Liew, K., Yu, J., 2013. Buckling analysis of functionally graded carbon nanotube-reinforced composite plates using the element-free kp-Ritz method. *Composite Structures*, 98, pp.160-168.